NANO LETTERS

pubs.acs.org/NanoLett

Letter

From Local to Collective Superconductivity in Proximitized Graphene

Stefano Trivini,* Tim Kokkeler, Jon Ortuzar, Eva Cortés-del Río, Beatriz Viña-Bausá, Pierre Mallet, Jean-Yves Veuillen, Juan Carlos Cuevas, Ivan Brihuega, F. Sebastian Bergeret, and Jose Ignacio Pascual*

Cite This: https://doi.org/10.1021/acs.nanolett.5c03487

Read Online

ACCESS | Metrics & More | Article Recommendations | Supporting Information

ABSTRACT: The superconducting proximity effect induces pairing correlations in metallic systems via Andreev scattering. This effect is particularly intriguing in graphene as it enables two-dimensional superconductivity that is tunable through doping. Understanding how superconducting correlations propagate within the metal is crucial to unveiling the key factors behind this tunability. Here, we employ scanning tunneling microscopy to investigate the energy and length scales of the proximity effect induced by Pb islands on graphene. Using tip-induced manipulation, we assemble S/N/S junctions with tunable N-region spacing and explore the evolution of the proximitized state in the confined normal region. We find that different doping levels can lead to either localized or collective superconducting states. By combining our experimental results with quasiclassical theory, we demonstrate that interface conductance plays a key role in determining the strength and coherence length of pairing correlations and interisland coupling. Our findings provide new insights into the design of novel superconducting states and the control of their properties.

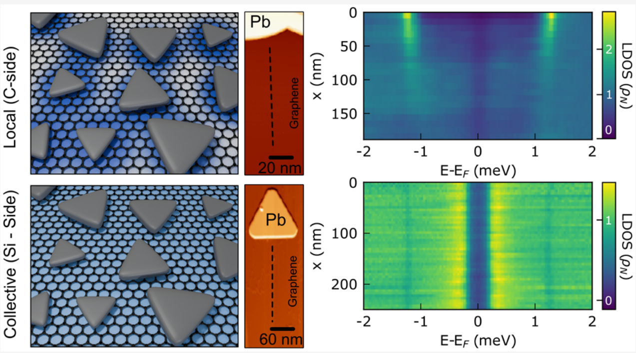

KEYWORDS: *superconductivity, scanning tunneling microscopy, proximity effect, graphene, island manipulation, collective superconductivity*

Superconducting pairing can be induced in normal metals (N) that are in good contact with a superconductor (S), where Andreev reflection governs electronic transfer across the interface.[1,2] This proximity effect is essential for inducing superconductivity in quantum materials, enabling a wide range of novel phases of matter and exotic effects, including unconventional pairing,[3−6] superconducting topological states,[7−9] nonreciprocal supercurrents,[10,11] and many-body correlations in magnetic impurities.[12−16]

The length scales of superconducting pairing propagation into N are crucial for transforming proximitized regions into a macroscopic superconducting state. In a normal region, the coherence length $\xi(E)$ can be much larger than the electron mean free path, justifying a diffusive description of the proximity effect.[17] It also depends inversely on the correlated electron/hole energy E, following the relation $\xi(E) = \sqrt{\hbar D/E}$, where D is the diffusion coefficient. Consequently, the normal local density of states (LDoS) in N is depleted over length scales ranging from $\xi(\Delta_S) = \sqrt{\hbar D/\Delta_S}$ at $E = \Delta_S$, the superconductor order parameter, to longer distances for $E \sim 0$. If N has a finite length d, the proximity effect induces a hard (mini)gap $\Delta_p \leq \Delta_S$, which is primarily determined by the Thouless energy $E_{Th} = \hbar D/d^2$.[18−25]

However, the efficiency of superconducting proximity is often limited by interface properties, frequently modeled by a transparency parameter that describes the balance between conventional electron scattering and Andreev reflection.[27] The interface transparency, usually parametrized by a dimensionless interface conductance ratio $\gamma = G_I/G_N$ of interface (I) and N,[28−30] plays a key role in determining the strength of pairing correlations in N and their characteristic length scales. Reducing the values of γ causes the narrowing of Δ_p and larger $\xi(\Delta_p)$ lengths.[31] Thus, understanding the role of the N/S interface in the proximity effect requires determining the size and shape of the proximity gap, as well as its dependence on length.[32] While scanning tunneling microscopy (STM) techniques have improved our ability to map the spatial dependence of the proximity-induced gap,[14,33−37] the experimental determination of γ remains elusive.

Received: July 4, 2025
Revised: October 3, 2025
Accepted: October 6, 2025

Here, we demonstrate that the strength and extension of the superconducting proximity effect in graphene can be controlled by the transparency of the superconductor−normal (S/N) interface. We compare STM measurements around Pb islands (S) grown on graphene (N) on the C- vs Si-terminated sides of a SiC crystal and observe striking differences in the induced superconducting state, as summarized in Figure 1a and 1b. On the C-side, the proximity effect is locally strong but spatially inhomogeneous, fading with distance from the islands; on the Si-side, the induced superconducting gap Δ_p is smaller yet extends homogeneously throughout the graphene layer, revealing a collective superconducting state. Through quasi-classical modeling of the proximity effect,[17,38−41] we attribute these different behaviors to variations in the S/N interface conductance γ. In particular, the weaker superconducting state induced on the Si-side shows longer coherence lengths, favoring a uniform proximity gap collectively determined by many islands. These findings establish the S/N interface conductance as a key parameter governing superconductivity in graphene-based hybrid systems.

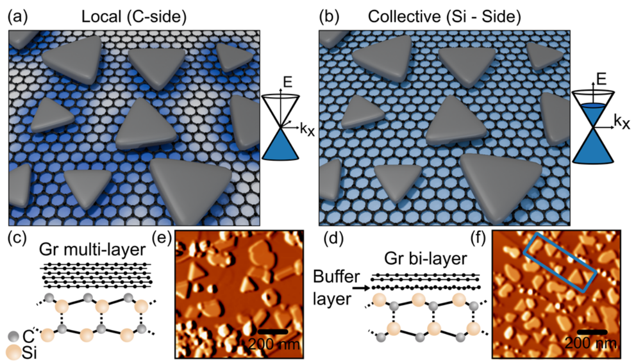

Figure 1. Local and collective proximity in SiC graphene. (a,b) Strength and distribution of superconductivity (in blue) induced by lead islands on graphene over the two sides of a SiC crystal with different native doping. Crystal structures of the (c) charge neutral graphene multilayer on the C-side and (d) the n-doped graphene bilayer on the Si side of a SiC crystal. (e,f) STM images of nanoscale Pb islands grown on graphene over the C-side and Si-side of a SiC crystal.[26] Tunnel parameters: V = 100 mV; I = 100 pA.

PREPARATION OF THE LEAD/GRAPHENE SYSTEM

Graphene layers can grow on the two surfaces of hexagonal silicon carbide crystals by annealing it to high temperatures.[42] As we show in the Supporting Information (SI[43]), graphene grows as a charge-neutral multilayer on the C-terminated SiC(000$\bar{1}$) side (*C-side*) and as an electron-doped bilayer on the Si-terminated SiC(0001), the *Si-side* [Figure 1c and 1d].[44] In two different experiments, we deposited lead (T_c = 7.2 K) by thermal sublimation on graphene on different sides of SiC crystals, at room temperature and under ultrahigh vacuum conditions. On both substrates, lead forms polygonal islands with lateral sizes of ∼50−200 nm and height of ∼3−10 nm (Figure 1e and 1f). To study the effect of Pb islands on the different graphene surfaces, we used a low-temperature scanning tunneling microscope at 1.2 K. We acquired differential conductance dI/dV spectra using Pb superconducting tips.[45−47] All spectra reported are deconvoluted to obtain the sample LDoS [details in SI[43]]. The Pb islands display a bulk-like BCS gap with two coherence peaks at Δ_S = 1.35 mV,

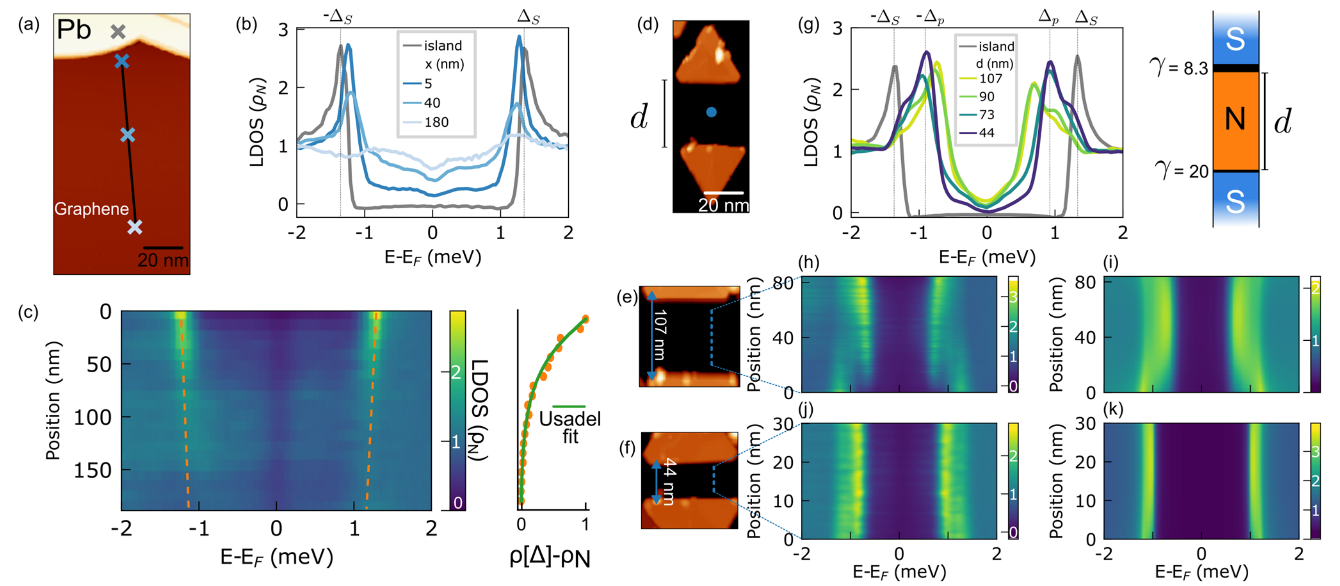

Figure 2. Proximitized superconductivity on C-side graphene. (a) STM image of a Pb island on top of C-side graphene. Line and crosses refer to the points at which the dI/dV spectroscopy in (b) and (c) are taken. (b) Deconvoluted dI/dV spectra (LDoS) measured on the crosses in (a). (c) Deconvoluted spatial dI/dV along the line in (a). Right, decay of the coherent peaks' amplitude with distance, fitted using Usadel equations for a N/S junction using ξ_S = 200 nm and Γ = 0.04 Δ. (d) STM image of an S/N/S junction built by lateral manipulation of two islands. (e) Zoomed-in image of the same junction at the 107 nm N-region. (f) Same junction after further STM-tip manipulation to the 44 nm N-region. (g) Deconvoluted dI/dV spectra at the center of the S/N/S junction for different island separations. (h) Deconvoluted spatial dI/dV in the 107 nm N-region. (i) Simulated LDoS of 107 nm S/N/S, with Δ = 1.35 mV, Γ = 0.04 Δ, ξ_S = 140 nm, d = 83 nm, top electrode γ = 8.3, and bottom electrode γ = 20. (j) Deconvoluted spatial dI/dV in the 44 nm long N-region. (k) Simulated LDoS of the 44 nm S/N/S. Parameters: Δ = 1.35 mV, Γ = 0.04 Δ, ξ_S = 140 nm, d = 30 nm, bottom electrode γ = 20, and top electrode γ = 8.3. STM topographies at V = 100 mV, I = 100 pA and dI/dV at V = 5 mV and I = 500 pA with δV = 100 uV lock-in modulation. Deconvolution was performed with Δ_t = 1.35 mV.

https://doi.org/10.1021/acs.nanolett.5c03487
Nano Lett. XXXX, XXX, XXX−XXX

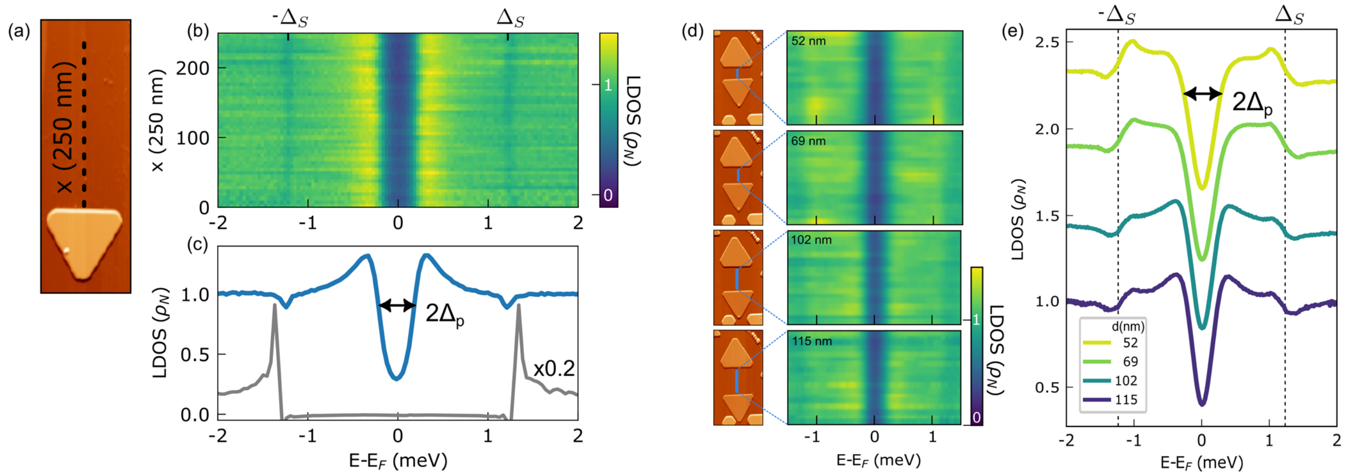

Figure 3. Proximity induced superconductivity on Si side graphene. (a) STM image of the region in Figure 1f with all islands removed except the one shown. (b) Spatial dependence of the LDoS in Si-side graphene along the dashed line in (a). (c) Deconvoluted dI/dV spectra measured on top of (gray, normalized for clarity) and near (blue) the island shown in panel (a). The minigap amounts to Δ_p = 0.2 mV. (d) Four snapshots of the closing of an S/N/S junction and deconvoluted dI/dV spectral profiles along the N region (blue lines in the images). (e) Deconvoluted dI/dV curves in the center or the S/N/S junction in (d). STM with V = 100 mV and I = 20pA; dI/dV set point: V = 6 mV; I = 600 pA. Deconvolution with Δ_t = 1.35 mV.

characteristic of Pb(111),[48] broadened by an inelastic term Γ = 0.04 Δ_S.

PROXIMITY EFFECT OF GRAPHENE ON C-SIDE SIC

We first investigate the proximity effect induced by Pb islands on the C-side graphene [Figure 2a], focusing on moiré-free domains that behave like free-standing graphene.[49,50] Spectra acquired near Pb islands display pronounced coherence peaks near $\pm\Delta_S$ [Figure 2b], which gradually diminish with distance from the islands [Figure 2c]. Such evolution of the LDoS in the N region is well-described by a one-dimensional quasiclassical model of an S/N system with an infinite N region, as detailed in ref 41. Applying the model to reproduce the spectral decay in Figure 2c, we obtain a coherence length $\xi_S = \xi(\Delta_S) \approx 200 \pm 10$ nm, consistent with previous reports,[34] and a diffusion coefficient $D \sim 820$ cm^2/s.

Graphene regions like the one in Figure 2a exhibit a net conductance for all subgap energies [Figure 2b], indicating incomplete proximitization, as expected for an infinite N region.[21] Surprisingly, graphene domain boundaries on the C-side, typically spaced with distances of a few times ξ_S,[51] do not induce minigaps inside the coherence peaks but at most faint zero-energy LDoS dips [Figure 2b]. This is probably remnant of a narrow gap smeared by finite temperature (1.2 K) or additional pair-breaking mechanisms, in line with low I_cR_n products observed in previous measurements.[52−55]

To induce a minigap in graphene, we confined N-regions between two Pb islands to lengths comparable to ξ_S. The S/N/S junction [Figure 2d] was created through STM tip manipulation[56−59] by laterally dragging triangular Pb islands to the desired positions.[36] Two Pb islands were initially positioned face to face on a moiré-free graphene region, separated by 107 nm [Figure 2e]. The spacing was gradually reduced to 44 nm by moving one island closer to the other using an STM tip [Figure 2f]. The spectral LDoS taken in the middle between the islands at each manipulation stage of 107, 90, 73, and 44 nm [Figure 2g] reveals the emergence of a proximity gap varying from ∼0.6 to 0.9 meV, and the in-gap conductance gradually decreases.

The wider S/N/S junction exhibits a spatially asymmetric LDoS [Figure 2h] with distinct proximity-induced gap values near the upper and lower islands. Since both islands have the same superconducting gap Δ_S and the Thouless energy E_{Th} is defined by the N region size, the asymmetry likely arises from variations in the transparency of the island−graphene interfaces. As shown in Figure 2i, this behavior is well captured by the 1D quasiclassical model, assuming a lower interface conductance for the top island (γ = 8.3) compared to the bottom one (γ = 20).

In contrast, the shorter S/N/S junction reveals a wider and more uniform proximity-induced gap along the N region [Figure 2j], with $\Delta_p \sim 0.9$ meV. The model in Figure 2k captures both the wider gap, consistent with a higher E_{Th}, and its homogeneity, even when using the same γ values as those for the more extended junction. This uniformity arises because the N region is much shorter than the superconducting coherence length. These results highlight the strong distance dependence of the proximity effect in graphene and the critical role of interface conductance in shaping proximity-induced minigaps.

PROXIMITY EFFECT OF GRAPHENE ON SI-SIDE SIC

On the Si-side of a SiC crystal, graphene proximitized by Pb islands—of similar size and number as those on the C-side—exhibits notable differences. The most striking is the presence of a pronounced minigap, homogeneously distributed all over the graphene sample. To illustrate this, we removed the surrounding islands around a selected one highlighted in Figure 1f. Probing the spectral evolution with distance from the selected island [Figure 3a], we remarkably find that the proximity gap remains spatially uniform over 250 nm [Figure 3b], in contrast to the local variations observed on the C-side in Figure 2c. The minigap has a width $\Delta_p \sim 0.2$ meV [Figure 3c], with faint dips at Δ_S = 1.3 meV, reminiscent of Pb island coherence peaks.

In contrast to the C-side, the LDoS shows lower signal at Δ_S both with and without confinement, the signal of a smaller γ

[see Figure S2 in SI[43]]. Moreover, in regions confined between two islands, the LDoS is relatively unperturbed. In the *tunable* S/N/S junction shown in Figure 3d, we compare the LDoS in the N region for island separations d = 115, 102, 69, and 52 nm and find that it stays nearly constant despite varying d. Even for separations below the reported $\xi_S \approx 150$ nm, rescaled to Δ_S from ref 34, the proximity gap retains the same width Δ_p as in other regions. The confinement induces only a slight increase in the LDoS near Δ_S, as is visible in the average spectra in Figure 3e.

The robustness of Δ_p upon island removal and its homogeneity around the sample suggests that, on the Si-side, the LDoS is not determined by individual island proximitization but rather by a collective effect involving all Pb islands over extended graphene regions, which stabilizes a global proximity gap.[60] Unraveling the origin of such differences requires extending the model to this configuration.

■ MODELING THE COLLECTIVE PROXIMITY EFFECT

The one-dimensional model used above cannot capture the collective proximity effect induced by multiple islands. Therefore, we adopt an island array configuration, shown in Figure 4a (see ref 43 for more details on the model), to solve the quasiclassical equations. The system consists of an infinite normal slab (N) proximitized by an array of superconducting islands (S) placed on top, with interface conductance γ and dimensions extracted from the experiments: island size l = 53 nm, spacing L = 106 nm, and superconducting coherence length ξ_S = 150 nm.[34]

For interface conductance γ = 6, the calculated LDoS along the N-slab shows a proximity-induced gap with strong spatial variations between the islands [Figure 4b], resembling the behavior on the C-side. Reducing γ yields smaller, more uniform gaps [Figure 4c], ultimately forming a nearly homogeneous minigap at γ = 0.75, with LDoS features at $E \sim \Delta_S$ washed out. This scenario seemingly reproduces the collective proximitization observed on the Si-side. As shown in Figure 4e, the model captures the LDoS features of the measured spectra in this multi-island regime.

The most striking feature of the Si-side proximity effect is the stability of the gap against confinement in an S/N/S junction [Figure 3d,e]. This behavior is not captured by the 1D model, which predicts the gap opening for any γ, but it is well explained by the array model. Simulating a tunable S/N/S junction with N-region length d embedded in a periodic array of Pb islands with spacing L, we reproduce the stability of the LDoS on d [Figure 4f]. As in the experiment, the proximity gap remains constant despite varying the d.

The array model also captures the enhanced spectral weight at Δ_S, as seen in the simulated LDoS spectra in Figure 4g. Furthermore, the collective nature of the superconducting state on the Si-side is confirmed by selectively removing Pb islands from the array, as demonstrated in the Figure S6 in SI.[43] This perturbation produces only slight changes in the proximity gap Δ_p, an effect accurately reproduced by the model.

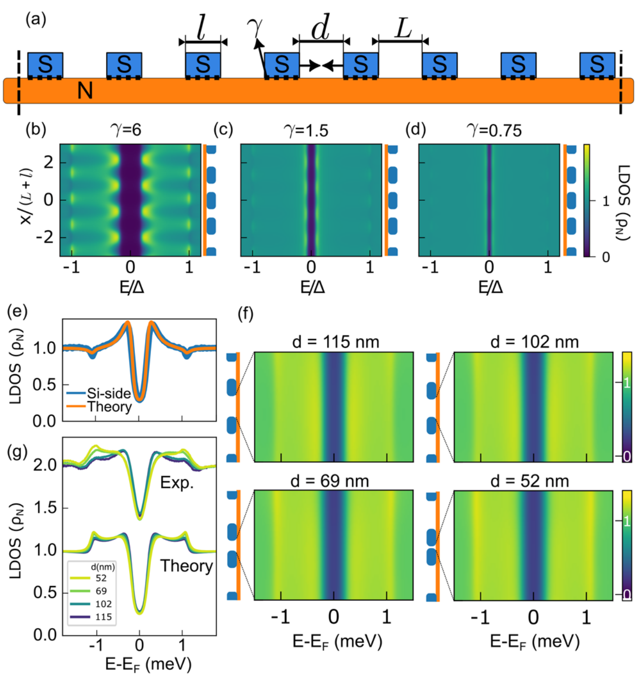

Figure 4. Simulation of a periodic array of islands. (a) Sketch of model used to simulate the proximity effect on the Si side, composed of a slab of normal metal with an array of islands in contact with it, extended with periodic boundary conditions. (b,c,d) LDoS along N slab for different interface conductance values γ = 6, 1.5, and 0.75, using ξ_S = 150 nm, $L = d$ = 300 nm, l = 150 nm, and $\Gamma = 0.04\ \Delta_S$. (e) The experimental LDoS on the Si-side from Figure 3b can be reproduced with the array model using parameters ξ_S = 150 nm, L = 300 nm, l = 100 nm, and γ = 3. (f) Calculated LDoS between two islands with different spacings d = 115, 102, 69, and 52 nm, keeping the remaining array in the unit cell with periodicity L = 106 nm and l = 53 nm and using ξ_S = 150 nm, γ = 1, and $\Gamma = 0.04\Delta_S$. (g) Calculated LDoS at the midpoint between the two central leads spaced by d in (f), qualitatively reproducing the experimental spectra presented in Figure 3d.

■ DISCUSSION

On the C-side, our results point to highly transparent interfaces, leading to intense coherence peaks at Δ_S and a large proximity-induced gap, which strongly depend on the size of the normal region. This aligns with the inverse dependence of the Thouless energy on the size of N, giving $\xi_S \sim 200$ nm at $E = \Delta_S = 1.35$ mV. In contrast, the Si-side shows a small, uniform proximity gap $\Delta_p \approx 0.2$ meV, about one-sixth of Δ_S, stable across the sample and in confined regions. The difference is attributed to significantly less transparent Pb—graphene interfaces.

The homogeneous LDoS on the Si-side reveals a collective superconducting state proximitized in the graphene layer. From the equation $\xi(E) = \sqrt{\hbar D/E}$, a smaller gap due to a more opaque interface results in a longer coherence length $\xi_{\Delta p}$. In fact, from the value $\xi_{\Delta p} \sim 600$ nm, rescaled to Δ_p from ref 34—about six times larger than the average interisland distance of 100 nm. Consequently, several tens of Pb islands can be proximity-coupled for the formation of a collective superconducting state, even without a periodic arrangement.[60,61] This results in a homogeneous spectral minigap across the sample. Modeling graphene as a single object proximitized by multiple islands captures the observed stability and uniformity of Δ_p—a hallmark of the collective proximity effect,[60,62,63] which persists even when removing most of the islands from a large graphene area [see Figure S5 in SI[43]].

Our results show that the S/N interface conductance is a key parameter that controls the proximity effect in graphene, which depends on the degree of doping. In particular, graphene has a similar work function as lead and, if electron-doped, results in larger interface dipoles and smaller tunneling rates compared to neutral graphene.[64] The graphene−metal separation also tends to increase with the degree of electron doping,[65] contributing to reducing the interface transparency. Based on this result, the uniformity of this superconducting state in graphene can be gate-controlled.[54,62]

■ ASSOCIATED CONTENT

Supporting Information

The Supporting Information is available free of charge at https://pubs.acs.org/doi/10.1021/acs.nanolett.5c03487.

Additional data and details about the theoretical model (PDF)

■ AUTHOR INFORMATION

Corresponding Authors

Stefano Trivini − *CIC nanoGUNE-BRTA, 20018 Donostia-San Sebastián, Spain;* orcid.org/0000-0001-8051-8683; Email: s.trivini@nanogune.eu

Jose Ignacio Pascual − *CIC nanoGUNE-BRTA, 20018 Donostia-San Sebastián, Spain; Ikerbasque, Basque Foundation for Science, 48009 Bilbao, Spain;* Email: ji.pascual@nanogune.eu

Authors

Tim Kokkeler − *Donostia International Physics Center (DIPC), 20018 Donostia-San Sebastián, Spain; University of Twente, 7522 NB Enschede, The Netherlands;* orcid.org/0000-0001-8681-3376

Jon Ortuzar − *CIC nanoGUNE-BRTA, 20018 Donostia-San Sebastián, Spain*

Eva Cortés-del Río − *Departamento de Física de la Materia Condensada, Universidad Autónoma de Madrid, 28049 Madrid, Spain; Department of Physics, University of Hamburg, 20355 Hamburg, Germany;* orcid.org/0000-0002-4422-8352

Beatriz Viña-Bausá − *CIC nanoGUNE-BRTA, 20018 Donostia-San Sebastián, Spain; Departamento de Física de la Materia Condensada, Universidad Autónoma de Madrid, 28049 Madrid, Spain;* orcid.org/0009-0007-3219-1680

Pierre Mallet − *Université Grenoble Alpes, CNRS, Institut Néel, 38042 Grenoble, France*

Jean-Yves Veuillen − *Université Grenoble Alpes, CNRS, Institut Néel, 38042 Grenoble, France*

Juan Carlos Cuevas − *Departamento de Física Teórica de la Materia Condensada and Condensed Matter Physics Center (IFIMAC), Universidad Autónoma de Madrid, 28049 Madrid, Spain;* orcid.org/0000-0001-7421-0682

Ivan Brihuega − *Departamento de Física de la Materia Condensada, Universidad Autónoma de Madrid, 28049 Madrid, Spain;* orcid.org/0000-0001-5032-9304

F. Sebastian Bergeret − *Centro de Física de Materiales (CFM-MPC), 20018 Donostia-San Sebastián, Spain; Donostia International Physics Center (DIPC), 20018 Donostia-San Sebastián, Spain*

Complete contact information is available at: https://pubs.acs.org/10.1021/acs.nanolett.5c03487

Notes

The authors declare no competing financial interest.

■ ACKNOWLEDGMENTS

We acknowledge financial support from the Spanish MCIN/AEI/10.13039/501100011033 and the European Regional Development Fund (ERDF) through grants PID2022-140845OB-C61, PID2023-148225NB-C31, PID2023-149106NB-I00, CEX2020-001038-M, CEX2023-001316-M, and TED2021-130292B-C42, from the Basque Government through grant IT-1591-22, from the European Union NextGenerationEU/PRTR-C17.I1 through the IKUR Strategy of the Department of Education of the Basque Government under a collaboration agreement with Ikerbasque MPC, CIC nanoGUNE, and DIPC, from the Comunidad de Madrid and the Spanish State through the Recovery, Transformation and Resilience Plan [Materiales Disruptivos Bidimensionales (2D), (MAD2DCM)-UAM Materiales Avanzados], and from the European Union's Horizon Europe through grant. J.O. acknowledges the scholarship PRE-2021-1-0350 from the Basque Government. B.V. acknowledges funding from the Spanish Ministerio de Universidades through the PhD scholarship No. FPU22/03675. E.C.R. acknowledges funding from the Alexander von Humboldt Foundation via the Henriette Herz program.

■ REFERENCES

(1) Andreev, A. F. The Thermal Conductivity of the Intermediate State in Superconductors. *JETP Lett.* **1964**, *19* (5), 1823−1828.

(2) Klapwijk, T. M. Proximity Effect From an Andreev Perspective. *J. Supercond.* **2004**, *17* (5), 593−611.

(3) Bergeret, F. S.; Volkov, A. F.; Efetov, K. B. Odd triplet superconductivity and related phenomena in superconductor-ferromagnet structures. *Rev. Mod. Phys.* **2005**, *77* (4), 1321−1373.

(4) Black-Schaffer, A. M.; Balatsky, A. V. Proximity-induced unconventional superconductivity in topological insulators. *Phys. Rev. B* **2013**, *87* (22), No. 220506.

(5) Cao, Y.; Fatemi, V.; Fang, S.; Watanabe, K.; Taniguchi, T.; Kaxiras, E.; Jarillo-Herrero, P. Unconventional superconductivity in magic-angle graphene superlattices. *Nature* **2018**, *556* (7699), 43−50.

(6) Balents, L.; Dean, C. R.; Efetov, D. K.; Young, A. F. Superconductivity and strong correlations in moiré flat bands. *Nat. Phys.* **2020**, *16* (7), 725−733.

(7) Leijnse, M.; Flensberg, K. Introduction to topological superconductivity and Majorana fermions. *Semicond. Sci. Technol.* **2012**, *27* (12), No. 124003.

(8) San-Jose, P.; Lado, J. L.; Aguado, R.; Guinea, F.; Fernández-Rossier, J. Majorana Zero Modes in Graphene. *Phys. Rev. X* **2015**, *5* (4), No. 041042.

(9) Frolov, S. M.; Manfra, M. J.; Sau, J. D. Topological superconductivity in hybrid devices. *Nat. Phys.* **2020**, *16* (7), 718−724.

(10) Ando, F.; Miyasaka, Y.; Li, T.; Ishizuka, J.; Arakawa, T.; Shiota, Y.; Moriyama, T.; Yanase, Y.; Ono, T. Observation of superconducting diode effect. *Nature* **2020**, *584* (7821), 373−376.

(11) Ilic, S.; Virtanen, P.; Crawford, D.; Heikkila, T. T.; Bergeret, F. S. Superconducting diode effect in diffusive superconductors and Josephson junctions with Rashba spin-orbit coupling. *Phys. Rev. B* **2024**, *110* (14), No. L140501.

(12) Kezilebieke, S.; Huda, M. N.; Vano, V.; Aapro, M.; Ganguli, S. C.; Silveira, O. J.; Głodzik, S.; Foster, A. S.; Ojanen, T.; Liljeroth, P. Topological superconductivity in a van der Waals heterostructure. *Nature* **2020**, *588* (7838), 424−428.

(13) Manna, S.; Wei, P.; Xie, Y.; Law, K. T.; Lee, P. A.; Moodera, J. S. Signature of a pair of Majorana zero modes in superconducting gold surface states. *Proc. Natl. Acad. Sci. U.S.A.* **2020**, *117* (16), 8775−8782.

(14) Stolyarov, V. S.; Pons, S.; Vlaic, S.; Remizov, S. V.; Shapiro, D. S.; Brun, C.; Bozhko, S. I.; Cren, T.; Menshchikova, T. V.; Chulkov,

E. V.; Pogosov, W. V.; Lozovik, Y. E.; Roditchev, D. Superconducting Long-Range Proximity Effect through the Atomically Flat Interface of a Bi $_2$ Te $_3$ Topological Insulator. *J. Phys. Chem. Lett.* **2021**, *12* (37), 9068−9075.

(15) Vaxevani, K.; Li, J.; Trivini, S.; Ortuzar, J.; Longo, D.; Wang, D.; Pascual, J. I. Extending the Spin Excitation Lifetime of a Magnetic Molecule on a Proximitized Superconductor. *Nano Lett.* **2022**, *22* (15), 6075−6082.

(16) Trivini, S.; Ortuzar, J.; Vaxevani, K.; Li, J.; Bergeret, F. S.; Cazalilla, M. A.; Pascual, J. I. Cooper Pair Excitation Mediated by a Molecular Quantum Spin on a Superconducting Proximitized Gold Film. *Phys. Rev. Lett.* **2023**, *130* (13), No. 136004.

(17) Usadel, K. D. Generalized Diffusion Equation for Superconducting Alloys. *Phys. Rev. Lett.* **1970**, *25* (8), 507−509.

(18) Fominov, Ya. V.; Feigel'man, M. V. Superconductive properties of thin dirty superconductor−normal-metal bilayers. *Phys. Rev. B* **2001**, *63* (9), No. 094518.

(19) Golubov, A. A.; Kupriyanov, M. Yu.; Il'ichev, E. The current-phase relation in Josephson junctions. *Rev. Mod. Phys.* **2004**, *76* (2), 411−469.

(20) Giazotto, F.; Peltonen, J. T.; Meschke, M.; Pekola, J. P. Superconducting quantum interference proximity transistor. *Nat. Phys.* **2010**, *6* (4), 254−259.

(21) Cherkez, V.; Cuevas, J. C.; Brun, C.; Cren, T.; Ménard, G.; Debontridder, F.; Stolyarov, V. S.; Roditchev, D. Proximity effect between two superconductors spatially resolved by scanning tunneling spectroscopy. *Phys. Rev. X* **2014**, *4* (1), 011033.

(22) Hijano, A.; Ilic, S.; Rouco, M.; Gonzalez-Orellana, C.; Ilyn, M.; Rogero, C.; Virtanen, P.; Heikkila, T. T.; Khorshidian, S.; Spies, M.; Ligato, N.; Giazotto, F.; Strambini, E.; Bergeret, F. S. Coexistence of superconductivity and spin-splitting fields in superconductor/ferromagnetic insulator bilayers of arbitrary thickness. *Phys. Rev. Res.* **2021**, *3* (2), No. 023131.

(23) Strambini, E.; Golovach, V. N.; De Simoni, G.; Moodera, J. S.; Bergeret, F. S.; Giazotto, F. Revealing the magnetic proximity effect in EuS/Al bilayers through superconducting tunneling spectroscopy. *Phys. Rev. Mater.* **2017**, *1* (5), No. 054402.

(24) Kashiwaya, S.; Ito, T.; Oka, K.; Ueno, S.; Takashima, H.; Koyanagi, M.; Tanaka, Y.; Kajimura, K. Tunneling spectroscopy of superconducting $Nd_{1.85}Ce_{0.15}CuO_{4-\delta}$. *Phys. Rev. B* **1998**, *57* (14), 8680−8686.

(25) Kashiwaya, S.; Tanaka, Y.; Koyanagi, M.; Takashima, H.; Kajimura, K. Origin of zero-bias conductance peaks in high-T_c superconductors. *Phys. Rev. B* **1995**, *51* (2), 1350−1353.

(26) Horcas, I.; Fernández, R.; Gómez-Rodríguez, J. M.; Colchero, J.; Gómez-Herrero, J.; Baro, A. M. WSXM: A software for scanning probe microscopy and a tool for nanotechnology. *Rev. Sci. Instrum.* **2007**, *78* (1), No. 013705.

(27) Blonder, G. E.; Tinkham, M.; Klapwijk, T. M. Transition from metallic to tunneling regimes in superconducting microconstrictions: Excess current, charge imbalance, and supercurrent conversion. *Phys. Rev. B* **1982**, *25* (7), 4515−4532.

(28) Kuprianov, M Yu; Lukichev, V. F. Influence of boundary transparency on the critical current of "dirty" SS'S structures. *Zh. Eksp. Teor. Fiz* **1988**, *94* (6), 139. http://jetp.ras.ru/cgi-bin/e/index/e/67/6/p1163?a=list.

(29) Belzig, W.; Bruder, C.; Schon, G. Local density of states in a dirty normal metal connected to a superconductor. *Phys. Rev. B* **1996**, *54* (13), 9443−9448.

(30) Hammer, J. C.; Cuevas, J. C.; Bergeret, F. S.; Belzig, W. Density of states and supercurrent in diffusive SNS junctions: Roles of nonideal interfaces and spin-flip scattering. *Phys. Rev. B* **2007**, *76* (6), No. 064514.

(31) Aminov, B. A.; Golubov, A. A.; Kupriyanov, M. Yu Quasiparticle current in ballistic constrictions with finite transparencies of interfaces. *Phys. Rev. B* **1996**, *53* (1), 365−373.

(32) Gueron, S.; Pothier, H.; Birge, N. O.; Esteve, D.; Devoret, M. H. Superconducting Proximity Effect Probed on a Mesoscopic Length Scale. *Phys. Rev. Lett.* **1996**, *77* (14), 3025−3028.

(33) le Sueur, H.; Joyez, P.; Pothier, H.; Urbina, C.; Esteve, D. Phase Controlled Superconducting Proximity Effect Probed by Tunneling Spectroscopy. *Phys. Rev. Lett.* **2008**, *100* (19), No. 197002.

(34) Natterer, F. D.; Ha, J.; Baek, H.; Zhang, D.; Cullen, W. G.; Zhitenev, N. B.; Kuk, Y.; Stroscio, J. A. Scanning tunneling spectroscopy of proximity superconductivity in epitaxial multilayer graphene. *Phys. Rev. B* **2016**, *93* (4), No. 045406.

(35) Cortes-del Rio, E.; Lado, J. L.; Cherkez, V.; Mallet, P.; Veuillen, J.-Y.; Cuevas, J. C.; Gomez-Rodriguez, J. M.; Fernandez-Rossier, J.; Brihuega, I. Observation of Yu-Shiba-Rusinov States in Superconducting Graphene. *Adv. Mater.* **2021**, *33* (22), No. 2008113.

(36) Cortes-del Rio, E.; Trivini, S.; Pascual, J. I.; Cherkez, V.; Mallet, P.; Veuillen, J.-Y.; Cuevas, J. C.; Brihuega, I. Shaping graphene superconductivity with nanometer precision. *Small* **2024**, *20* (20), No. 2308439.

(37) Trivini, S.; Ortuzar, J.; Vaxevani, K.; Vina-Bausá, B.; Bergeret, F. S.; Pascual, J. I. Local Control of Parity and Charge in Nanoscale Superconducting Lead Islands. *arXiv*, 2025, https://arxiv.org/abs/2507.12150.

(38) Larkin, A. I.; Ovchinnikov, Y. N. Quasiclassical method in the theory of superconductivity. *Sov Phys. JETP* **1969**, *28* (6), 1200−1205. http://jetp.ras.ru/cgi-bin/e/index/e/28/6/p1200?a=list.

(39) Eilenberger, G. Transformation of Gorkov's equation for type II superconductors into transport-like equations. *Zeitschrift für Physik A Hadrons and nuclei* **1968**, *214*, 195−213.

(40) Golubov, A. A.; Kupriyanov, M. Y. Kupriyanov. Theoretical investigation of Josephson tunnel junctions with spatially inhomogeneous superconducting electrodes. *Journal of Low Temperature Physics* **1988**, *70* (1), 83−130.

(41) Virtanen, P.; Heikkilä, T. T. Thermoelectric effects in superconducting proximity structures. *Appl. Phys. A: Mater. Sci. Process.* **2007**, *89*, 625.

(42) Norimatsu, W.; Kusunoki, M. Epitaxial graphene on SiC{0001}: Advances and perspectives. *Phys. Chem. Chem. Phys.* **2014**, *16* (8), 3501.

(43) SI.

(44) Luxmi; Srivastava, N.; He, G.; Feenstra, R. M.; Fisher, P. J. Comparison of graphene formation on C-face and Si-face SiC {0001} surfaces. *Phys. Rev. B* **2010**, *82* (23), No. 235406.

(45) Rodrigo, J. G.; Suderow, H.; Vieira, S. On the use of STM superconducting tips at very low temperatures. *European Physical Journal B - Condensed Matter and Complex Systems* **2004**, *40* (4), 483−488.

(46) Franke, K. J.; Schulze, G.; Pascual, J. I. Competition of Superconducting Phenomena and Kondo Screening at the Nanoscale. *Science* **2011**, *332* (6032), 940−944.

(47) Pillet, J-D.; Quay, C. H. L.; Morfin, P.; Bena, C.; Yeyati, A. L.; Joyez, P. Andreev bound states in supercurrent-carrying carbon nanotubes revealed. *Nat. Phys.* **2010**, *6* (12), 965−969.

(48) Ruby, M.; Heinrich, B. W.; Pascual, J. I.; Franke, K. J. Experimental demonstration of a two-band superconducting state for lead using scanning tunneling spectroscopy. *Phys. Rev. Lett.* **2015**, *114* (15), No. 157001.

(49) Hass, J.; Varchon, F.; Millán-Otoya, J. E.; Sprinkle, M.; Sharma, N.; de Heer, W. A.; Berger, C.; First, P. N.; Magaud, L.; Conrad, E. H. Why Multilayer Graphene on 4 H - SiC(000 $\bar{1}$) Behaves Like a Single Sheet of Graphene. *Phys. Rev. Lett.* **2008**, *100* (12), No. 125504.

(50) Sprinkle, M.; Siegel, D.; Hu, Y.; Hicks, J.; Tejeda, A.; Taleb-Ibrahimi, A.; Le Fèvre, P.; Bertran, F.; Vizzini, S.; Enriquez, H.; Chiang, S.; Soukiassian, P.; Berger, C.; de Heer, W. A.; Lanzara, A.; Conrad, E. H. First direct observation of a nearly ideal graphene band structure. *Phys. Rev. Lett.* **2009**, *103* (22), No. 226803.

(51) Varchon, F.; Mallet, P.; Magaud, L.; Veuillen, J.-Y. Rotational disorder in few-layer graphene films on 6 H - Si C(000 - 1): A scanning tunneling microscopy study. *Phys. Rev. B* **2008**, *77* (16), No. 165415.

https://doi.org/10.1021/acs.nanolett.5c03487
Nano Lett. XXXX, XXX, XXX−XXX

(52) Heersche, H. B.; Jarillo-Herrero, P.; Oostinga, J. B.; Vandersypen, L. M. K.; Morpurgo, A. F. Bipolar supercurrent in graphene. *Nature* **2007**, *446* (7131), 56−59.
(53) Komatsu, K.; Li, C.; Autier-Laurent, S.; Bouchiat, H.; Gueron, S. Superconducting proximity effect in long superconductor/graphene/superconductor junctions: From specular Andreev reflection at zero field to the quantum Hall regime. *Phys. Rev. B* **2012**, *86* (11), No. 115412.
(54) Han, Z.; Allain, A.; Arjmandi-Tash, H.; Tikhonov, K.; Feigel'man, M.; Sacepe, B.; Bouchiat, V. Collapse of superconductivity in a hybrid tin-graphene Josephson junction array. *Nat. Phys.* **2014**, *10* (5), 380−386.
(55) Li, C.; Gueron, S.; Chepelianskii, A.; Bouchiat, H. Full range of proximity effect probed with superconductor/graphene/superconductor junctions. *Phys. Rev. B* **2016**, *94* (11), No. 115405.
(56) Eigler, D. M.; Schweizer, E. K. Positioning single atoms with a scanning tunnelling microscope. *Nature* **1990**, *344* (6266), 524−526.
(57) Schneider, L.; Ton, K. T.; Ioannidis, I.; Neuhaus-Steinmetz, J.; Posske, T.; Wiesendanger, R.; Wiebe, J. Proximity superconductivity in atom-by-atom crafted quantum dots. *Nature* **2023**, *621* (7977), 60−65.
(58) Rutten, L. M.; Schmid, H.; Liebhaber, E.; Franceschi, G.; Yazdani, A.; Reecht, G.; Rossnagel, K.; von Oppen, F.; Franke, K. J. Wave Function Engineering on Superconducting Substrates: Chiral Yu-Shiba-Rusinov Molecules. *ACS Nano* **2024**, *18* (44), 30798−30804.
(59) Trivini, S.; Ortuzar, J.; Zaldivar, J.; Herrera, E.; Guillamon, I.; Suderow, H.; Bergeret, F. S.; Pascual, J. I. Diluted Yu-Shiba-Rusinov arrays on the anisotropic superconductor β-Bi_2Pd. *Phys. Rev. B* **2024**, *110* (23), No. 235405.
(60) Feigel'man, M. V.; Skvortsov, M. A.; Tikhonov, K. S. Proximity-induced superconductivity in graphene. *JETP Lett.* **2008**, *88* (11), 747−751.
(61) Kessler, B. M.; Girit, Ç. Ö.; Zettl, A.; Bouchiat, V. Tunable Superconducting Phase Transition in Metal-Decorated Graphene Sheets. *Phys. Rev. Lett.* **2010**, *104* (4), No. 047001.
(62) Eley, S.; Gopalakrishnan, S.; Goldbart, P. M.; Mason, N. Approaching zero-temperature metallic states in mesoscopic superconductor-normal-superconductor arrays. *Nat. Phys.* **2012**, *8* (1), 59−62.
(63) Chen, F.; Liu, Y.; Guo, W.; Wang, T.; Tian, Z.; Zhang, M.; Xue, Z.; Mu, G.; Zhang, X.; Di, Z. Quantum Griffiths Singularity in Ordered Artificial Superconducting-Islands-Array on Graphene. *Nano Lett.* **2024**, *24* (8), 2444−2450.
(64) Mammadov, S.; Ristein, J.; Krone, J.; Raidel, C.; Wanke, M.; Wiesmann, V.; Speck, F.; Seyller, T. Work function of graphene multilayers on SiC(0001). *2D Mater.* **2017**, *4* (1), No. 015043.
(65) Giovannetti, G.; Khomyakov, P. A.; Brocks, G.; Karpan, V. M.; Van Den Brink, J.; Kelly, P. J. Doping Graphene with Metal Contacts. *Phys. Rev. Lett.* **2008**, *101* (2), No. 026803.

https://doi.org/10.1021/acs.nanolett.5c03487
Nano Lett. XXXX, XXX, XXX−XXX